Inhibition of the heat shock protein 90 molecular chaperone *in vitro* and *in vivo* by novel, synthetic, potent resorcinylic pyrazole/isoxazole amide analogues

Swee Y. Sharp,[1] Chrisostomos Prodromou,[2] Kathy Boxall,[1] Marissa V. Powers,[1] Joanna L. Holmes,[1] Gary Box,[1] Thomas P. Matthews,[1] Kwai-Ming J. Cheung,[1] Andrew Kalusa,[1] Karen James,[1] Angela Hayes,[1] Anthea Hardcastle,[1] Brian Dymock,[3] Paul A. Brough,[3] Xavier Barril,[3] Julie E. Cansfield,[3] Lisa Wright,[3] Allan Surgenor,[3] Nicolas Foloppe,[3] Roderick E. Hubbard,[3] Wynne Aherne,[1] Laurence Pearl,[2] Keith Jones,[1] Edward McDonald,[1] Florence Raynaud,[1] Sue Eccles,[1] Martin Drysdale,[3] and Paul Workman[1]

[1]Cancer Research UK Centre for Cancer Therapeutics, The Institute of Cancer Research, Haddow Laboratories, Sutton, Surrey, United Kingdom; [2]Section of Structural Biology, The Institute of Cancer Research, Chester Beatty Laboratories, London, United Kingdom; and [3]Vernalis Ltd., Granta Park, Great Abington, Cambridge, United Kingdom

Abstract

Although the heat shock protein 90 (HSP90) inhibitor 17-allylamino-17-demethoxygeldanamycin (17-AAG) shows clinical promise, potential limitations encourage development of alternative chemotypes. We discovered the 3,4-diarylpyrazole resorcinol CCT018159 by high-throughput screening and used structure-based design to generate more potent pyrazole amide analogues, exemplified by VER-49009. Here, we describe the detailed biological properties of VER-49009 and the corresponding isoxazole VER-50589. X-ray crystallography showed a virtually identical HSP90 binding mode. However, the dissociation constant (K_d) of VER-50589 was 4.5 ± 2.2 nmol/L compared with 78.0 ± 10.4 nmol/L for VER-49009, attributable to higher enthalpy for VER-50589 binding. A competitive binding assay gave a lower IC_{50} of 21 ± 4 nmol/L for VER-50589 compared with 47 ± 9 nmol/L for VER-49009. Cellular uptake of VER-50589 was 4-fold greater than for VER-49009. Mean cellular antiproliferative GI_{50} values for VER-50589 and VER-49009 for a human cancer cell line panel were 78 ± 15 and 685 ± 119 nmol/L, respectively, showing a 9-fold potency gain for the isoxazole. Unlike 17-AAG, but as with CCT018159, cellular potency of these analogues was independent of NAD(P)H:quinone oxidoreductase 1/DT-diaphorase and P-glycoprotein expression. Consistent with HSP90 inhibition, VER-50589 and VER-49009 caused induction of HSP72 and HSP27 alongside depletion of client proteins, including C-RAF, B-RAF, and survivin, and the protein arginine methyltransferase PRMT5. Both caused cell cycle arrest and apoptosis. Extent and duration of pharmacodynamic changes in an orthotopic human ovarian carcinoma model confirmed the superiority of VER-50589 over VER-49009. VER-50589 accumulated in HCT116 human colon cancer xenografts at levels above the cellular GI_{50} for 24 h, resulting in 30% growth inhibition. The results indicate the therapeutic potential of the resorcinylic pyrazole/isoxazole amide analogues as HSP90 inhibitors. [Mol Cancer Ther 2007;6(4):1198–211]

Introduction

The abundant 90-kDa molecular chaperone heat shock protein 90 (HSP90) is associated both with stress responses and with the folding, stabilization, activation, and biological function of many important oncogenic client proteins such as steroid hormone receptors and protein kinases (1, 2). An updated list of client proteins is available online.[4] The major advantage of targeting HSP90 is the simultaneous combinatorial depletion of multiple proteins involved in the hallmark traits of cancer (3), thereby blocking malignant progression at multiple levels and reducing the likelihood of drug resistance arising (4). Therapeutic selectivity for cancer versus normal cells might be achieved by exploiting oncogene addiction (4). In addition, mutated oncoproteins are often hypersensitive to HSP90 inhibition (5, 6), and chaperone dependence of tumors is increased by the fact

Received 3/5/07; revised 3/13/07; accepted 3/14/07.

Grant support: Cancer Research UK [CUK] programme grants C309/A2187 and C309/A8274, Wellcome Trust, and Vernalis Ltd.

The costs of publication of this article were defrayed in part by the payment of page charges. This article must therefore be hereby marked *advertisement* in accordance with 18 U.S.C. Section 1734 solely to indicate this fact.

Note: P. Workman is a Cancer Research UK Life Fellow. J. Holmes is funded by a studentship from Cancer Research UK.

Requests for reprints: Paul Workman, Cancer Research UK Centre for Cancer Therapeutics, The Institute of Cancer Research, Haddow Laboratories, 15 Cotswold Road, Belmont, Sutton, Surrey, SM2 5NG, United Kingdom. Phone: 44-20-8722-4301; Fax: 44-20-8722-4324. E-mail: Paul.Workman@icr.ac.uk

doi:10.1158/1535-7163.MCT-07-0149

[4] http://www.picard.ch

that cancer cells are stressed by the effects of oncogenes and microenvironmental factors (2). Furthermore, HSP90 in cancer cells is reported to exist in a superchaperone complex that is much more sensitive to HSP90 inhibition than the uncomplexed form that predominates in normal cells (7).

HSP90 activity is regulated by numerous co-chaperones and is driven by a cycle of NH_2-terminal ATP/ADP exchange and ATP hydrolysis (8, 9). Inhibition of HSP90 ATPase activity targets client proteins for proteasomal degradation (10, 11). Several natural products act as potent HSP90 inhibitors (e.g., geldanamycin and radicicol; Fig. 1) but exhibited *in vivo* toxicity and/or stability issues (12, 13), restricting their suitability for clinical development. The less toxic geldanamycin derivative 17-allylamino-17-demethoxygeldanamycin (17-AAG; Fig. 1) is in phase II clinical trials but is difficult to formulate, has low oral bioavailability, is subject to polymorphic metabolism by cytochrome P450 CYP3A4 (14) and NAD(P)H:quinone oxidoreductase 1 (NQO1/DT-diaphorase; refs. 15, 16), and is effluxed by P-glycoprotein (15). Although the 17-dimethylaminoethylamino analogue 17-DMAG (Fig. 1) is more soluble and orally bioavailable, it showed similar preclinical toxicities to 17-AAG (17). The 17-AAG hydroquinone IPI-504 has high aqueous solubility and has entered phase I clinical trial but is converted to the potentially toxic quinone 17-AAG (18). Compared with radicicol itself, semisynthetic oxime derivatives of radicicol exhibited increased solubility and improved antitumor properties in murine models (19) but have not yet progressed to the clinic.

Given the promising results with the natural product derivatives, alternative HSP90 inhibitor chemotypes, particularly synthetic small molecules, are of considerable interest (20–22). The natural product inhibitors block HSP90 by binding to the NH_2-terminal ATP site (23). Based on X-ray crystal structures of HSP90 bound to various ligands (23), Chiosis et al. designed purine scaffold HSP90 inhibitors (24). These were optimized into purines with good solubility, oral bioavailability, and *in vivo* activity (24). A purine scaffold agent (CNF-2024) has entered clinical trial (25).

We discovered our novel, synthetic 3,4-diarylpyrazole resorcinol HSP90 inhibitor CCT018159 by high-throughput screening (Fig. 1; refs. 26, 27). Pharmacokinetics of early analogues were characterized by cassette dosing (28). Structure-based design generated more potent analogues, particularly the amides exemplified by the pyrazole VER-49009 (CCT0129397; Fig. 1; ref. 29). Here, we describe the detailed biological properties of VER-49009 and the corresponding isoxazole analogue VER-50589 (CCT0130024; Fig. 1). As seen from their chemical structures, VER-49009 and VER-50589 differ only in the pyrazole versus isoxazole heterocycle. The pyrazole to isoxazole switch does not affect the critical hydrogen bonding network exhibited by the pyrazole resorcinol unit that anchors this class of inhibitors to the HSP90 NH_2-terminal ATP site (26, 27, 29), while also avoiding steric changes that would not be tolerated. We show here that the isoxazole has greater binding affinity than the corresponding pyrazole and also exhibits enhanced cellular uptake, leading to more potent HSP90 inhibition and antiproliferative

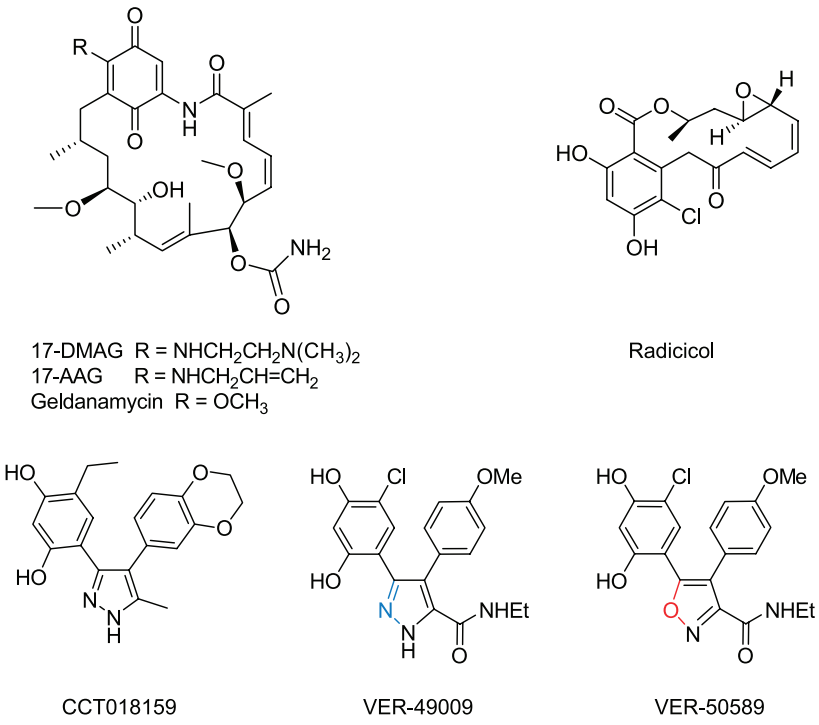

Figure 1. Chemical structures of HSP90 inhibitors. Structural differences between the pyrazole VER-49009 (*blue*) and the corresponding isoxazole VER-50589 (*red*) are highlighted.

activity in cells. In addition, we report pharmacokinetic and pharmacodynamic properties that are sufficient to give rise to what is, to our knowledge, the first published report of *in vivo* therapeutic activity with the pyrazole/isoxazole resorcinol HSP90 inhibitors. VER-50589 exhibits the tightest binding of any small molecule synthetic HSP90 inhibitor yet reported. It compares favorably with the clinically evaluated drug 17-AAG, illustrates the value of structure-based design and optimization, and exhibits potential for further enhancement to produce a clinical development candidate.

Materials and Methods

Compounds

VER-49009 and VER-50589 were synthesized as described (29, 30). 17-AAG was from Axxora Ltd. (Nottingham, United Kingdom). The NQO1 inhibitor ES936 was kindly provided by Prof. Chris Moody (University of Nottingham, United Kingdom). Compounds were dissolved in DMSO.

Cell Culture

Unless otherwise stated, cell lines were from the American Type Culture Collection (LGC Promochem, Middlesex, United Kingdom) and cultured as described (27). Penicillin (100 units/mL) and streptomycin (100 μg/mL; Invitrogen, Paisley, United Kingdom) were added to the medium for human breast cancer cells. Human umbilical vein endothelial cells (HUVEC) and the nontumorigenic cell lines MCF10a (human mammary gland) and PNT2 (human prostate epithelial cells immortalized with SV40) were from the European Collection of Animal Cell Cultures (Wiltshire, United Kingdom) and cultured as described (27). All lines were screened routinely for *Mycoplasma* (Venor GeM kit, Minerva Biolabs, Berlin, Germany).

Protein Production and X-ray Crystallography

Protein production, crystallization, and X-ray crystallography were done as described (27, 29, 31).

Isothermal Titration Calorimetry

The dissociation constant (K_d) for HSP90 inhibitor binding was measured by isothermal titration calorimetry with 10 μmol/L full-length recombinant human HSP90β (23).

Determination of HSP90 ATPase Activity

Inhibition of the intrinsic ATPase activity of full-length recombinant yeast Hsp90 or of the full-length recombinant human HSP90β in the presence of the activator AHA1 (32) was measured by the malachite green assay (33).

Fluorescence Polarization Assay

Binding of HSP90 inhibitors to human full-length recombinant HSP90β was determined by a competitive binding fluorescence polarization assay, using a fluorescent pyrazole resorcinol probe (34).

Cell Proliferation Assay

Antiproliferative effects were measured using the sulforhodamine B assay (15, 27). HUVEC sensitivity was determined by an alkaline phosphatase method (35).

In vitro Cell Uptake

HCT116 and HT29 human colon cancer cells were seeded and left to attach overnight. Vehicle control or compound was added for 1, 4, and 24 h. Attached cells were collected and counted by hemacytometer. Incubation medium (1 mL) and cell pellets were frozen at −80°C until mass spectrometry analysis (see later).

Western Blotting

Procedures for cell lysates and Western blotting were as described (27). Antibodies used are listed in Supplementary Materials.[5]

Cell Cycle Analysis

Cell cycle effects were determined using propidium iodide staining and flow cytometry (36).

Apoptosis Studies

Attached and trypan blue–negative detached cells were counted using a hemacytometer. Poly(ADP-ribose) polymerase cleavage was detected by Western blotting using an antibody (Clontech, Oxford, United Kingdom) that recognizes the 116-kDa native poly(ADP-ribose) polymerase and the 85-kDa apoptosis-related cleavage product (36).

Human Tumor Xenografts

All work was done in accordance with UK Home Office regulations under the Animals (Scientific Procedures) Act 1986 and according to UK Co-ordinating Committee on Cancer Research guidelines for animal experimentation (37) with local Ethical Committee approval.

Compounds were dissolved in DMSO and diluted in sterile saline/Tween 20 such that mice received the dose required in 0.1 mL of final solution per 10 g body weight. Final concentrations were 10% DMSO, 5% Tween 20, 85% saline. Controls received an equal volume of vehicle only.

For pharmacokinetic studies, athymic mice were administered either 20 mg/kg of compound i.v. or 200 mg/kg i.p. Plasma and tumor samples were collected as described (38), snap frozen, and stored at −80°C before analysis.

HCT116 cells (2–5 million cells per site) were injected s.c. in the flanks of 6- to 8-week-old female NCr athymic mice. Dosing commenced when tumors were well established (~5–6 mm diameter). For combined therapy and pharmacokinetic and pharmacodynamic studies, mice bearing HCT116 xenografts were administered 100 mg/kg VER-50589 i.p. per day for 9 days. Tumor volumes were calculated (39). On study termination, blood samples were taken, and plasma was separated and stored −80°C. Tumors were excised, weighed, and snap frozen at −80°C.

In some studies, female NCr athymic mice were implanted i.p. with 10 million OVCAR3 ovarian carcinoma cells harvested from donor mice. This tumor mimics late-stage malignant disease (40). Once tumors were well established (day 37 after passage, as evidenced by increased abdominal girth), mice were injected i.p. with 4 mg/kg VER-49009 or VER-50589 twice daily over 2 days (four doses total). Tumors were harvested at intervals after the last dose and snap frozen for pharmacodynamic analyses.

Pharmacokinetic Analysis

Tumors were homogenized in 3 mL PBS/g of tumor. Control, plasma, and tumor (100 μL) were analyzed for compound levels following protein precipitation with

[5] Supplementary materials for this article are available at Molecular Cancer Therapeutics Online (http://mct.aacrjournals.org/).

3 volumes of methanol containing an analogue as internal standard. Quantitative analysis of plasma and tumors was done by liquid chromatography tandem mass spectrometry (see Supplementary Materials).[5]

Pharmacodynamic Analysis

Tumor samples were homogenized into a fine powder under liquid nitrogen using a model 6750 freezer mill (Glen Crestor, Stanmore, United Kingdom; see Supplementary Materials).[5] Western blotting was done as above. Induction of HSP72 was quantified by ELISA (41).

Statistical Analysis

All values are mean ± SE. Statistical significance was calculated by *t* tests for the *in vitro* experiments and Mann-Whitney *U* test for human xenograft studies. $P < 0.05$ was considered statistically significant.

Results

X-ray Protein Crystallography

Information gained from the X-ray co-crystal structure of our high-throughput screening hit compound CCT018159 bound to NH_2-terminal yeast HSP90 (26) led to the design of more potent analogues, particularly the diarylpyrazole amides (29). The binding of VER-49009 to the NH_2-terminal domain of recombinant human HSP90α is shown in Fig. 2A. This confirms the crucial network of hydrogen bonding interactions involving the resorcinol residue and pyrazole ring with Asp^{93}, Thr^{184} and a cluster of structurally conserved and highly ordered water molecules, as reported for CCT018159 (26, 29). In addition, the C-5 ethylamide residue adds further hydrogen bond interactions with the protein backbone via Lys^{58} and Gly^{97}, the latter in particular contributing to the enhanced potency of VER-49009 over previous compounds lacking the amide group (29). Replacement of the central pyrazole in VER-49009 with an isoxazole gave VER-50589 (Fig. 1) and the co-crystal structure with NH_2-terminal human HSP90α is shown in Fig. 2B. The similarity of binding mode is immediately apparent, with the pyrazole VER-49009 and the isoxazole VER-50589 making essentially identical interactions in the nucleotide-binding pocket (Fig. 2A and B). Figure 2C shows two orthogonal views of the superimposition of VER-49009, VER-50589, and ADP. It can be seen that VER-49009 and VER-50589 bind with overall similarity to ADP but with some differences in their relative spatial arrangement within the binding pocket (Fig. 2C).

HSP90 ATPase Inhibitory and Binding Activities

IC_{50} values for inhibition of the intrinsic ATPase activity, as measured by malachite green assay at 400 μmol/L ATP using full-length recombinant yeast Hsp90, were 167 ± 9 nmol/L for VER-49009 and 143 ± 23 nmol/L for VER-50589. IC_{50} values were higher for inhibition of human full-length recombinant human HSP90β in the presence of the activator AHA1 (1,033 ± 88 and 821 ± 12 nmol/L for VER-49009 and VER-50589, respectively). Using the much more sensitive competitive binding assay, the IC_{50} value for VER-50589 was 21 ± 4 nmol/L, which was 2-fold lower than that for VER-49009 (IC_{50} = 47 ± 9 nmol/L).

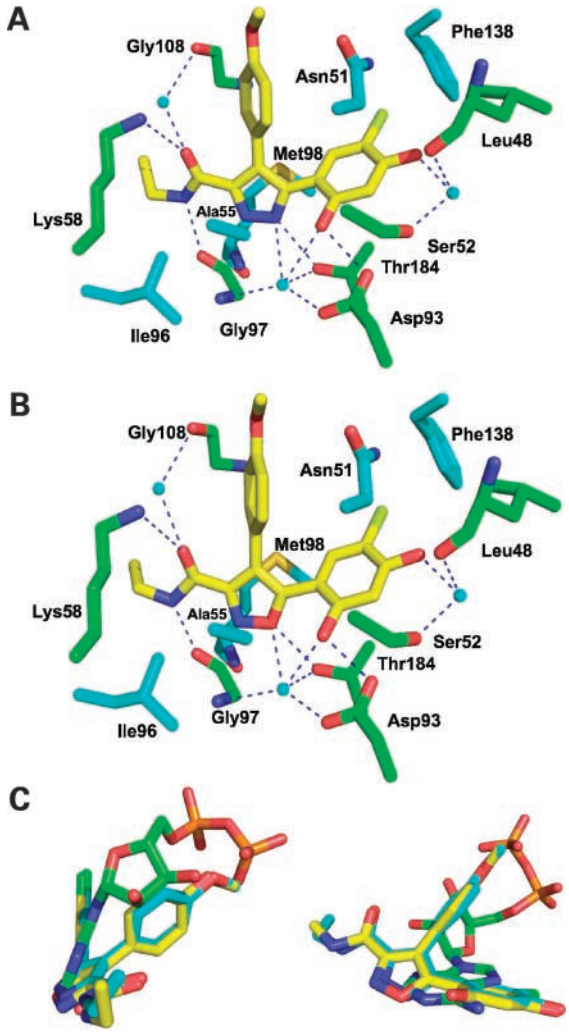

Figure 2. Pymol diagrams showing binding interactions between the ATP-binding site of human HSP90α and (**A**) VER-49009 and (**B**) VER-50589. Hydrogen bonds (*dotted blue lines*), amino acid residues involved (*green*), water molecules (*cyan-colored spheres*), and residues in van der Waals contact (*cyan*). **C,** orthogonal views of the bound structures of VER-49009 (*cyan*), VER-50589 (*yellow*), and ADP (*green*), overlaid by superimposition of the HSP90 NH_2-domains from the crystal structures of the individual complexes. Protein X-ray crystallography was determined at 2.1- and 2.0-Å resolution for VER-49009 and VER-50589, respectively. Coordinates and structure factors have been deposited in the Protein Data Bank under 2BSM for VER-49009 and 2UWD for VER-50589.

Interestingly, the dissociation constant (K_d) for the binding of the isoxazole VER-50589 to the full-length recombinant human HSP90β, as measured by isothermal titration calorimetry, was 17-fold lower than that for the pyrazole VER-49009 (4.5 ± 2.2 and 78.0 ± 10.4 nmol/L, respectively). The K_d values indicate that the isoxazole VER-50589 binds more tightly to the protein under the conditions used. The isothermal titration calorimetry measurements reveal that the enthalpy change (ΔH) on binding the pyrazole VER-49009 is −6.41 kcal/mol, whereas the ΔH for the binding of the isoxazole

VER-50589 is higher at −9.36 kcal/mol. The entropy changes (ΔS) are 11.4 and 7.1 cal/mol/K, respectively. Although all these values are favorable, the higher value for the enthalpy of binding of VER-50589 is likely to be the major contributor to the increased binding affinity as measured by K_d.

Antiproliferative Activity in Human Cancer Cells

The cellular potency of the isoxazole VER-50589 was consistently higher when compared with the pyrazole VER-49009 in all the human cancer cell lines tested (Table 1A). The GI_{50} values for the isoxazole ranged from 1.3-fold (SKMEL 5 melanoma) to 33.6-fold (BT-474 breast cancer) lower than those for the pyrazole, with the lowest GI_{50} seen in CH1 human ovarian cells (32.7 ± 0.2 nmol/L). Mean values for the cancer cell panel were 78 ± 15 nmol/L for VER-50589 versus 685 ± 119 nmol/L for VER-49009 (P = 0.0001), showing a 9-fold greater potency for VER-50589.

Cell Uptake and Metabolism

As with CCT018159 (27), there was considerable cellular accumulation of both VER-50589 and VER-49009 in HCT116 human colon cancer cells (Table 2A). Interestingly, the isoxazole showed 4-fold more cellular accumulation than the pyrazole after 24 h of exposure to equimolar concentrations (Table 2A). Together with lower K_d for HSP90 binding, the greater uptake of VER-50589 compared

Table 1.

A. Cellular GI_{50} values for VER-49009 and VER-50589 in a panel of human cancer cell lines and nontumorigenic cells *in vitro*, as measured by sulforhodamine B assay

Cell type	Cell line	GI_{50} (nmol/L)	
		VER-49009	VER-50589
Melanoma	SKMEL 2	1,093.3 ± 111.2	62.0 ± 4.3
	SKMEL 5	163.3 ± 14.5	125.0 ± 22.6
	SKMEL 28	475.0 ± 18.0	45.3 ± 4.2
	WM266.4	1,366.7 ± 33.3	55.3 ± 5.8
Colon cancer	HCT116	357.0 ± 0.003	115 ± 0.005
	BEneg	372.5 ± 29.5	36.7 ± 2.7
	BE2*	422.5 ± 46.2	35.0 ± 3.5
	HT29	4,600.0 ± 611.0	1,115.0 ± 95.2
	HT29oxaliR†	4,300.0 ± 602.8	666.7 ± 118.5
Ovarian cancer	CH1	376.7 ± 26.0	32.7 ± 0.3
	CH1doxR‡	436.7 ± 21.9	39.3 ± 0.7
Breast cancer	MB-231	570.0 ± 0.04	58.8 ± 6.4
	MB-468	490.0 ± 0.04	38.0 ± 4.8
	BT20	550.0 ± 0.09	59.0 ± 12.7
	ZR751	1,030.0 ± 0.1	134.7 ± 28.7
	MCF7	1,360.0 ± 0.2	197.3 ± 74.1
	BT-474	390.0 ± 0.01	11.6 ± 0.4
Endothelial cells	HUVEC	444.0 ± 91.1	19.0 ± 2.4
Breast epithelium	MCF10a	1,660.0 ± 152.1	330.0 ± 84.1
Prostate epithelium	PNT2	1,720.5 ± 942.0	179.5 ± 50.1

B. Effects of the potent NQO1 inhibitor ES936 (0.5 μmol/L) on the sensitivity of BEneg (null NQO1) and BE2 (high NQO1) human colon cancer cell lines, as measured by sulforhodamine B assay

Compound	Cell line	GI_{50} (nmol/L)	
		Control	With ES936
17-AAG	BEneg	253.3 ± 18.6	256.7 ± 8.8
	BE2	36.0 ± 4.6	270.0 ± 11.6
VER-49009	BEneg	523.3 ± 3.3	496.7 ± 8.8
	BE2	660.0 ± 23.1	580.0 ± 30.6
VER-50589	BEneg	42.3 ± 1.9	42.0 ± 1.2
	BE2	60.7 ± 0.7	57.0 ± 3.6

NOTE: Values are mean ± SE of n = 3 to 4 (A) and n = 3 (B).
*Transfected with the *NQO1* gene for DT-diaphorase (43).
† Acquired resistance to oxaliplatin (45).
‡ Acquired resistance to doxorubicin, high levels of P-glycoprotein (44).

Table 2.

A. Cellular accumulation of VER-50589 and VER-49009 in the HCT116 human colon cancer cells (cells were exposed to compounds at 357 nmol/L)

Time (h)	Concentration (nmol/10^6 cells)	
	VER-50589	VER-49009
1	0.056	0.014
4	0.062	0.014
24	0.118	0.031

B. Cellular concentrations of VER-50589 and VER-49009 and their respective glucuronide metabolites in HT29 human colon cancer cells (cells were exposed to compounds at 4,600 nmol/L)

Time (h)	Concentration of parent and glucuronide (nmol/10^6 cells)			
	VER-50589		VER-49009	
	Parent	Glucuronide	Parent	Glucuronide
1	0.015	0.168	0.013	1.280
4	0.010	0.254	0.020	1.620
24	0.011	0.120	0.002	0.090

C. Concentrations of glucuronide metabolites of VER-50589 and VER-49009 in tissue culture medium following treatment of HT29 human colon cancer cells with VER-50589 or VER-49009 (cells were exposed to compounds at 4,600 nmol/L)

Time (h)	Concentration of glucuronide in tissue culture medium (nmol/L)	
	VER-50589	VER-49009
1	443	415
4	3,050	1,639
24	3,994	1,757

D. Percentage of VER-50589 and VER-49009 metabolized in mouse liver microsomes following 5, 15, and 30 min of incubation of 10 μmol/L compound in 200 μL of 1 mg/mL microsomal protein

Time (min)	% Metabolized	
	VER-50589	VER-49009
5	79 ± 5	71 ± 17
15	100	100
30	100	100

NOTE: Values are mean ± SE of $n = 3$.

with VER-49009 seems likely to contribute to the difference in cellular potency between the two resorcinols.

Extensive glucuronidation of the resorcinol hydroxyl groups in CCT018159 was seen in HT29 but not HCT116 human colon cancer cells (27). There was similarly extensive glucuronidation of VER-50589 and VER-49009 in HT29 cells (glucuronide levels of 50- to 230-fold higher than those of the respective parent compounds intracellularly; Table 2B) but not in HCT116 cells (glucuronide levels >50-fold lower than the respective parent compounds; data not shown). Glucuronidation and the resulting lower parent compound levels is likely to be responsible for the resistance of HT29 cells to these HSP90 inhibitors (Table 1A). There may be a difference between VER-50589 and VER-49009 with respect to metabolism and/or the subsequent disposition of metabolites in HT29 cells as the glucuronides of the two agents are distributed differently between cells and tissue culture medium (Table 2B and C). However, the greater uptake in HCT116 cells of VER-50589 compared with VER-49009 cannot be explained by a difference in metabolism of the two compounds as HCT116 cells do not express uridine diphosphoglucuronosyltransferases (42), and there was no difference in their microsomal metabolism (Table 2D).

Antiproliferative Activity in HUVECs and Nontumorigenic Cells

VER-49009 and VER-50589 inhibited HUVEC proliferation with GI_{50} values of 444 ± 91.1 and 19 ± 2.4 nmol/L, respectively. This indicates similar (for VER-49009) or greater sensitivity (for VER-50589) of HUVEC compared with tumor cells (Table 1A). However, the nontumorigenic human breast (MCF10a) and prostate (PNT2) epithelial cells exhibited higher GI_{50} values for VER-49009 and VER-50589 when compared with their respective mean GI_{50} values against cancer cells.

Effects of NQO1/DT-Diaphorase on Cellular Sensitivity

Cellular activity of 17-AAG is dependent on the levels of NQO1/DT-diaphorase due to NQO1-mediated reduction to the more potent hydroquinone (15, 16). The melanoma cell lines used here express varying NQO1 levels, with SKMEL 5 and WM266.4 exhibiting the highest activity, SKMEL 28 showing intermediate activity, and SKMEL 2 exhibiting the lowest level (15). Cellular sensitivity to the pyrazole/isoxazole resorcinol HSP90 inhibitors showed no association with NQO1 levels. To further confirm this, we compared the BEneg human colon carcinoma cell line that lacks NQO1 activity due to an inactivating NQO1 polymorphism and the BE2 line that was transfected with the wild-type *NQO1* gene and shows high level of expression (43). Unlike 17-AAG (43) and similar to CCT018159 (27), VER-49009 and VER-50589 exhibited no differences in cellular activities between these isogenic cell lines ($P = 0.5$; Table 1A).

We also tested the effects of the mechanism-based inhibitor of NQO1, 5-methoxy-1,2-dimethyl-3-([4-nitrophenoxy]ethyl)indole-4,7-dione (ES936; ref. 16), on the sensitivity of cancer cells to the HSP90 inhibitors. As shown previously (15, 27), increased sensitivity of 17-AAG was observed in the BE2 line with high NQO1 levels (Table 1B). Cellular sensitivity to 17-AAG in the BE2 line was markedly reduced by the NQO1 inhibitor, whereas that of the isogenic BEneg NQO1-negative line was unaffected. Indeed, ES936 effectively abrogated the differential effect of 17-AAG in the isogenic pair. In contrast to 17-AAG, sensitivity to VER-49009 or VER-50589 exhibited no significant differences ($P = 0.2$) in the presence or absence of ES936 (Table 1B). These results clearly indicate that the cellular activities of the pyrazole/isoxazole resorcinol compounds are independent of NQO1 expression.

Growth-Inhibitory Effects in Cell Lines with Acquired Drug Resistance

The multidrug resistant efflux protein P-glycoprotein confers resistance to 17-AAG, as seen in the NCI 60 human cancer cell line panel (15) and using a human ovarian carcinoma cell line made resistant to doxorubicin, CH1doxR (27, 44). Unlike 17-AAG but in common with CCT018159 (27), VER-49009 and VER-50589 each exhibited similar cellular GI_{50} values in CH1doxR compared with parental CH1 cells (Table 1A). In addition, the multidrug resistance reversal agent *R*-verapamil did not alter the GI_{50} values of VER-49009 or VER-50589 ($P = 0.9$; data not shown). Table 1A also shows that VER-49009 and VER-50589 exhibited no differences ($P = 0.7$) in their cellular activity in HT29 human colon cancer cells versus its acquired oxaliplatin-resistant counterpart (Table 1A; ref. 45). These results suggest that the pyrazole/isoxazole resorcinols are not P-glycoprotein substrates and are able to circumvent resistance to oxaliplatin.

Effects on Molecular Biomarkers

The molecular signature of HSP90 inhibition has been well established in cancer cell lines, validated in human tumor xenografts, and used to show target inhibition in cancer patients receiving 17-AAG (15, 46). Pharmacologic concentrations of 17-AAG caused increased expression of HSP72 and depletion of oncogenic client proteins, such as ERBB2, cyclin-dependent kinase 4, and C-RAF, in human melanoma and breast and colon cancer cells (27, 36, 47). Similar results were observed with equivalent growth-inhibitory concentrations of VER-49009 and VER-50589 in human melanoma and breast cancer cells; likewise, treatment with VER-49009 or VER-50589 induced HSP72 and HSP27 (Fig. 3A and B; Supplementary Fig. S1).[5] Both are up-regulated at least in part by the transcription factor heat shock factor-1 (48, 49).

The kinetics of client protein depletion were similar for VER-49009 and VER-50589 in the SKMEL 2 (Fig. 3A) and WM266.4 melanoma cells (Supplementary Fig. S1).[5] Depletion of the well-established client proteins, in particular ERBB2, C-RAF, and cyclin-dependent kinase 4, was observed (Fig. 3A; Supplementary Fig. S1).[5] Phosphorylated AKT was also depleted to a greater extent and more rapidly than the total AKT protein levels (phosphorylated plus non–phosphorylated AKT1, AKT2, and AKT3). Although AKT is a client of HSP90, our studies are consistent with those of others in showing that total AKT was generally depleted much later than many other client proteins and that depletion was variable between cell lines. It has been shown that the reduction in phosphorylated AKT upon HSP90 inhibition is due to the increase in protein phosphatase 2A–mediated dephosphorylation (50). Extracellular signal-regulated kinases 1 and 2 (ERK1/2) are not client proteins, and the reduction in their levels of phosphorylation is a result of depletion of the upstream RAF proteins (see below). Similar results were observed when BT20 human breast cancer cells were treated with VER-50589 (Fig. 3B). No change in the molecular biomarkers were observed with inactive analogues (27).

Melanoma cells are commonly driven by the RAS/RAF/mitogen-activated protein kinase kinase (MEK1/2)/ERK1/2 pathway (51). SKMEL 2 and WM266.4 cells have wild-type B-RAF and mutant ^{V600D}B-RAF, respectively (27). Compared with the wild-type, mutant B-RAF was more sensitive to 17-AAG and the pyrazole resorcinol CCT018159 (5, 6, 27). VER-49009 and VER-50589 depleted B-RAF as early as 8 h in both SKMEL 2 and WM266.4 cells (Fig. 3A and Supplementary Fig. S1,[5] respectively). In

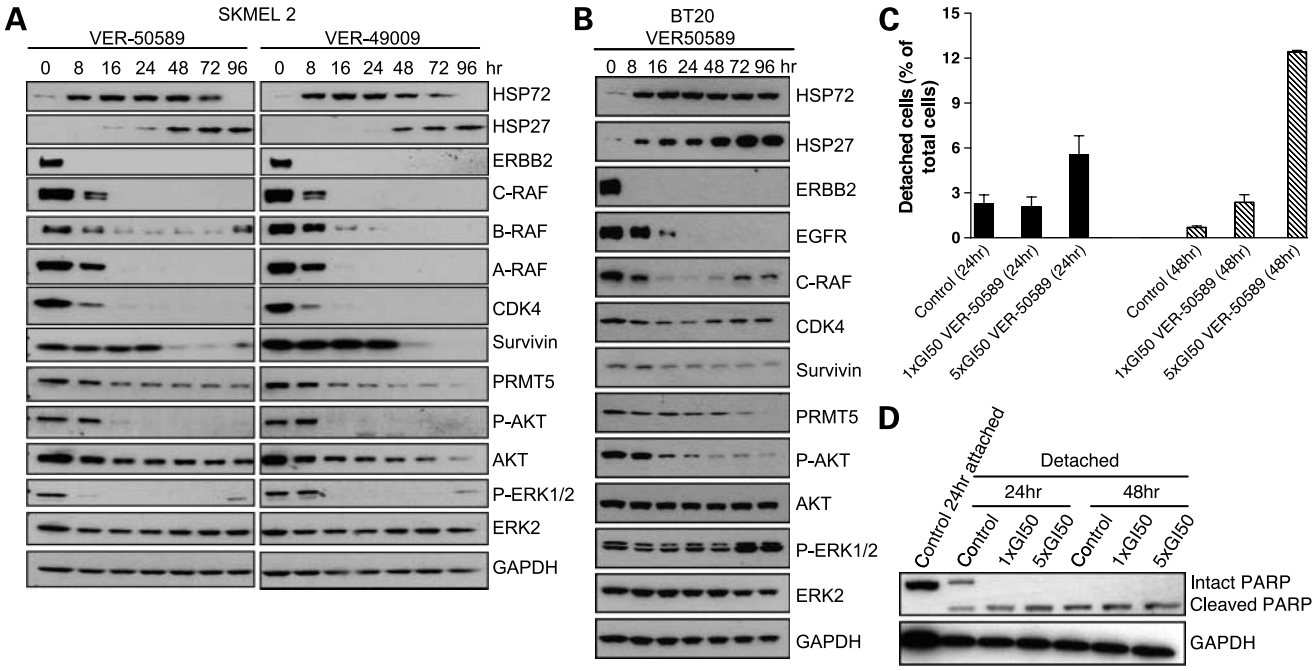

Figure 3. Effects of VER-49009 and VER-50589 on molecular biomarkers and apoptosis. **A,** Western blot of lysates from SKMEL 2 human melanoma cells treated with 5 × GI_{50} concentrations of VER-49009 (5,467 nmol/L), VER-50589 (310 nmol/L), or vehicle control over 96 h. **B,** Western blot of BT20 human breast cancer cells treated with 5 × GI_{50} concentration of VER-50589 (247 nmol/L) over 96 h. **C,** detached HCT116 cells (expressed as % total cells) following treatment with 1 and 5 × GI_{50} concentrations of VER-50589 (115 and 575 nmol/L, respectively) or vehicle control for 24 and 48 h. **D,** poly(ADP-ribose) polymerase (PARP) cleavage detected by Western blot in the detached HCT116 cells following treatment with 1 and 5 × GI_{50} concentrations of VER-50589 or vehicle control for 24 and 48 h. The poly(ADP-ribose) polymerase antibody recognizes the 116-kDa native poly(ADP-ribose) polymerase and the 85-kDa apoptosis-related cleavage product. Note that although poly(ADP-ribose) polymerase cleavage is seen in the detached sample of both control and treated populations, both HSP90 inhibitors caused an increase in the number of detached, apoptotic cells (see **C**). Glyceraldehyde-3-phosphate dehydrogenase (GAPDH) was used as loading control. EGFR, epidermal growth factor receptor; CDK4, cyclin-dependent kinase 4; P-AKT, phosphorylated AKT; P-ERK1/2, phosphorylated extracellular signal-related kinase.

addition to B-RAF and C-RAF (see above), A-RAF was also depleted. As mentioned above, decreased ERK1/2 phosphorylation is seen as a downstream consequence of RAF depletion.

ERBB2 is consistently the most sensitive HSP90 client protein, in terms of both the rate of its disappearance (Fig. 3A and B) and also the concentration-response relationship, with depletion seen at 1 × GI_{50} concentrations of VER-49009 and VER-50589 (Supplementary Fig. S2).[5] Another ERBB family member, epidermal growth factor receptor, was depleted in the BT20 breast carcinoma line (Fig. 3B).

Additional, less frequently studied HSP90 client proteins were also depleted. VER-49009 and VER-50589 depleted the inhibitor of apoptosis protein survivin in SKMEL 2 and WM266.4 melanoma cells and BT20 breast cancer cells (Fig. 3A and B; Supplementary Fig. S1A).[5] Using proteomic analysis, we previously identified the protein arginine methyltransferase PRMT5 to be a novel HSP90 binding and client protein that was depleted by 17-AAG (52). VER-49009 and VER-50589 also depleted PRMT5 (Fig. 3A and B; Supplementary Fig. S1).[5]

Cell Cycle Arrest, Cytostasis, and Apoptosis

17-AAG and CCT018159 cause G_1 and G_2-M cell cycle arrest and induce cytostasis and apoptosis (27, 36). We therefore investigated these responses with VER-49009 and VER-50589. Both agents caused a G_1 and G_2-M block in HCT116 colon cancer cells as early as 8 h, and this was sustained over 48 h (data not shown). When HCT116 cells were treated with 1 and 5 × GI_{50} concentrations of VER-50589 (115 or 575 nmol/L, respectively), concentration-dependent cytostasis was observed up to 48 h (Supplementary Fig. S3).[5] VER-50589 also caused an increase (2.4- and 17.7-fold after 24 and 48 h, respectively, at 5 × GI_{50} concentrations) in trypan blue–negative detached cells when compared with control (Fig. 3C). At 1 × GI_{50} concentration, there was no difference after 24 h in detached cells when compared with controls, but a 3.4-fold increase was seen after 48 h. Poly(ADP-ribose) polymerase cleavage was detected at both concentrations after 24 and 48 h in the detached HCT116 cell population, consistent with apoptosis (Fig. 3D). Apoptosis was also seen when WM266.4 cells were treated with VER-50589 (data not shown).

Pharmacokinetics in Mice

The plasma concentration versus time profiles in athymic mice following i.v. administration of 20 mg/kg VER-49009 or VER-50589 are shown in Fig. 4A. Pharmacokinetic parameters were similar for the two compounds. Both showed rapid clearance with values of 0.187 and 0.272 L/h

A

Compound	Cmax (nmol/L)	AUClast (hr*nmol/L)	AUCINF_obs (hr*nmol/L)	HL_ Lambda_z (hr)	CL-obs (L/hr)	Vss_obs (L)
VER-49009	23953	5507	5515	0.205	0.187	0.040
VER-50589	15891	3776	3790	0.284	0.272	0.066

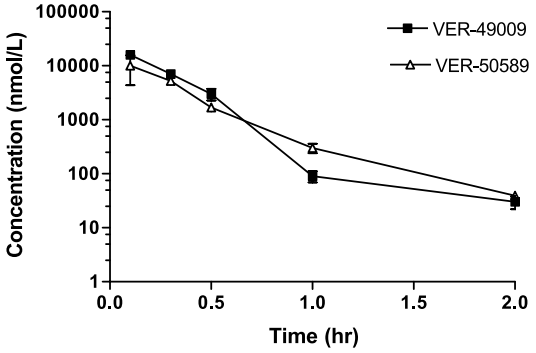

B

Tissue	Tmax (hr)	Cmax (nmol/L)	HL_ Lambda_z (hr)	AUClast (hr*nmol/L)	AUCINF_obs (hr*nmol/L)	VZ_F-obs (L)	CL_F_obs (L/hr)
Plasma	0.5	11358	0.997	10312.5	10336.9	1.435	0.997
Tumor	0.5	6758	5.693	50098.3	53539.1	1.582	0.193

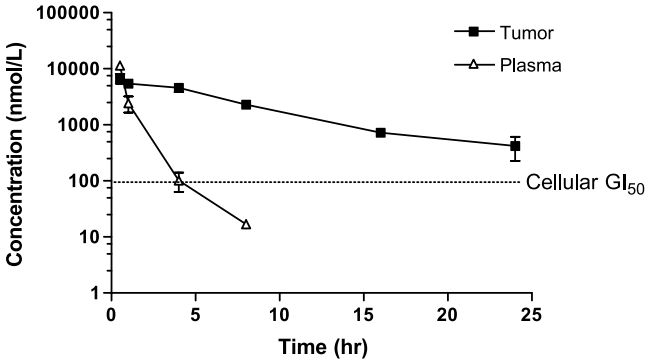

Figure 4. Pharmacokinetics of VER-49009 and VER-50589. **A,** plasma concentration versus time profiles following i.v. administration of 20 mg/kg VER-49009 or VER-50589 in athymic mice bearing HCT116 human colon carcinoma xenografts. Pharmacokinetic parameters calculated with WinNonlin are summarized in the table and are similar for both compounds. **B,** plasma and tumor levels were determined following i.p. administration of the higher dose of 200 mg/kg VER-50589. Pharmacokinetic parameters were calculated with WinNonlin and are summarized in the table for both plasma and tumor tissue. Mean of two independent repeats.

for the pyrazole and isoxazole, respectively, values that exceed mouse liver blood flow (0.108 L/h). The elimination half-lives of both compounds were relatively short (~0.2–0.3 h). Due to rapid clearance, plasma concentrations exceeded the cellular GI_{50} for only 1 h for both compounds. Given the higher cell uptake (Table 2A) and lower cellular GI_{50} levels (Table 1A) for VER-50589 compared with VER49009, the isoxazole was selected for further pharmacokinetic evaluation in tumor-bearing animals.

Following i.p. administration of 200 mg/kg VER-50589 to athymic mice bearing HCT116 human colon carcinoma xenografts, the terminal half-life was ~1 h (Fig. 4B). The isoxazole was detected in plasma up to 6 h after dosing (Fig. 4B). It distributed rapidly into tumor tissue where it accumulated with a tumor to plasma ratio of 5 and a half-life of 5.7 h. This accumulation is consistent with the cell uptake studies described earlier. Thus, tumor VER-50589 levels exceeded the cellular GI_{50} for 24 h after dosing.

In vivo Pharmacodynamic Changes and Efficacy in Human Tumor Xenografts

Given the promising tumor exposures described in the previous section, we wished to evaluate the potential to achieve pharmacodynamic changes consistent with HSP90 inhibition and to obtain an indication of *in vivo* efficacy. Initial studies were carried out to determine the depletion of the sensitive HSP90 client protein ERBB2 following a short course of VER-50589 or VER-49009 delivered i.p. to human ovarian cancer cells growing orthotopically in the peritoneal cavity. Following administration of four doses of

only 4 mg/kg i.p. to athymic mice bearing well-established OVCAR3 human ovarian ascites tumors, VER-49009 induced clear depletion of ERBB2 at 3 and 8 h following the final dose, with client protein levels returning to normal by 24 h (Fig. 5A, *top*). Consistent with its more favorable binding potency and cell uptake properties described earlier, VER-50589 induced a more complete HSP90 inhibition, which was maintained at 24 h (Fig. 5A, *bottom*). The isoxazole was, therefore, selected for subsequent studies in a human solid tumor model.

To determine the ability of systemically administered compound to affect the growth of established solid tumors, mice bearing s.c. HCT116 colon carcinoma xenografts (mean volume, 150 mm^3) received nine daily doses of 100 mg/kg i.p. VER-50589. This schedule was well tolerated with no body weight loss (data not shown). Control tumors excised at the end of the study had a median volume of 650 $\pm$ 40 mm^3 compared with 456 $\pm$ 38 mm^3 for those treated with VER-50589 (30% tumor volume inhibition, $n = 19$, $P = 0.0153$). The corresponding mean tumor weights were 390 $\pm$ 22.5 mg in the controls compared with 290 $\pm$ 25.2 mg in the treated (26% tumor weight loss, $P = 0.04$). Tumor extracts showed clear up-regulation of HSP72 in response to VER-50589 at 8, 16, and 24 h after the last dose, as measured by quantitative ELISA (Fig. 5B). Tumor levels of VER-50589 at the end of the experiment were very similar to those following a single administration, indicating no further accumulation or induction of metabolism with multiple dosing (data not shown).

In an independent study, mice bearing established HCT116 xenografts were treated with the same schedule of VER-50589 or vehicle, and samples were obtained for more detailed pharmacodynamic analysis. Figure 5C shows decreased expression of ERBB2 and C-RAF in the treated tumors, consistent with inhibition of HSP90 at doses causing tumor growth inhibition.

Discussion

HSP90 is a target of considerable interest for the development of rational cancer therapy due to its chaperoning of multiple oncogenic client proteins and its role in supporting all of the hallmark traits of cancer cells (4). Clinical evaluation of 17-AAG, the first HSP90 inhibitor to enter the clinic, showed target inhibition and an indication of clinical activity at a manageable level of toxicity (46). Preclinical and clinical results have also shown the limitations of this drug (see Introduction). Identification of novel HSP90 inhibitor classes with improved structural characteristics and better pharmacologic profiles is therefore of major interest (21, 22). We discovered the 3,4-diarylpyrazole resorcinol class of HSP90 inhibitor, exemplified by CCT018159, by high-throughput screening (26) and characterized its biological properties (27). Subsequently, we used structure-based design to produce more potent inhibitors, as illustrated by the amide pyrazole resorcinols such as VER-49009 (29). Here, we describe the detailed biological properties of the pyrazole VER-49009 and of the corresponding isoxazole VER-50589. These two compounds differ only in the replacement of the pyrazole nitrogen in VER-49009 by the isoxazole oxygen in VER-50589 (Fig. 1).

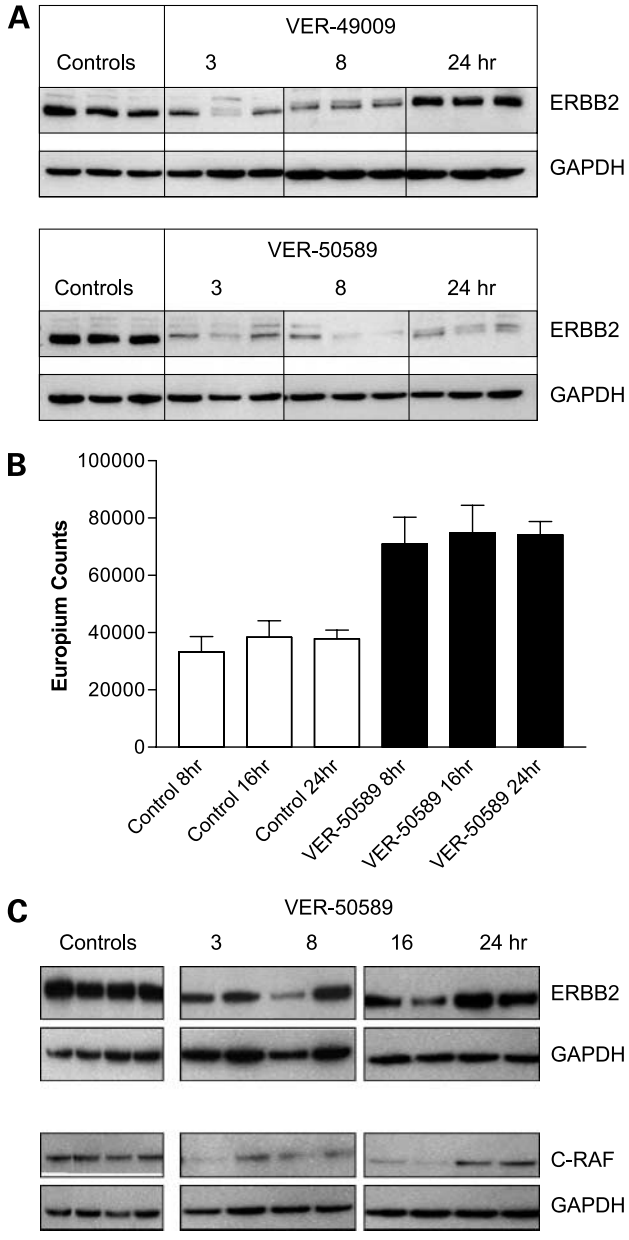

Figure 5. Effects of VER-49009 and VER-50589 on HSP72 induction and client protein depletion *in vivo*. **A,** athymic mice bearing well-established OVCAR3 human ovarian ascites tumors were injected i.p. at a dose of 4 mg/kg twice daily over 2 d (total of four doses) of VER-49009 and VER-50589. Samples were from mice receiving vehicle or compounds collected at 3, 8, and 24 h following the final dose for detection of ERBB2 client protein in tumor lysates by Western blotting. **B,** mice bearing s.c. HCT116 colon carcinoma xenografts were dosed with 100 mg/kg VER-50589 i.p. daily for 9 d, as in the tumor therapy studies (see text). Tumors were excised and snap frozen after 8, 16, and 24 h after final dose. The induction of HSP72 was quantified in tumor lysates by ELISA. **C,** as for **B**, depletion of ERBB2 and C-RAF in tumor lysates was detected by Western blotting. Glyceraldehyde-3-phosphate (GAPDH) was used as the loading control in all Westerns in this figure.

X-ray co-crystal structures showed a virtually identical binding mode for VER-49009 and VER-50589, involving key hydrogen bond interactions and water molecules. When compared with the equivalent structure for CCT018159 (26, 29), further hydrogen bond interactions with Lys^{58} and Gly^{97} in the protein backbone of human HSP90α were achieved with the ethylamide residue of VER-49009 and VER-50589, the latter interaction in particular contributing to enhanced target and cellular potencies. All of the resorcinylic pyrazole/isoxazoles exhibit the same essential anchoring mechanism in which critical hydrogen bond interactions are formed between the ligand and Asp^{93}, Thr^{184}, and key water molecules at the base of the nucleotide binding pocket.

The dissociation constant (K_d) for the isoxazole VER-50589 was 17-fold lower than that of VER-49009. The increase in binding affinity of VER-50589 is largely due to the higher value for the enthalpy of binding for the isoxazole. Although the arrangements of O and N atoms involved in the binding of VER-49009 and VER-50589 to HSP90 appear very similar from a crystallographic point of view (Fig. 2), the more favorable enthalpy of VER-50589 binding may indicate that the actual strength of hydrogen bond interactions is greater for isoxazole VER-50589. The variation in bond energy of a hydrogen bond with distance between the donor and the acceptor can be considerable and such subtle bond length changes may be beyond the resolution of the crystal structure determinations. An alternative explanation is that the pyrazole, unlike the isoxazole, can exist in two tautomeric forms. If the tautomer bound to the protein is not the ground state tautomer, then an energetic penalty must be paid for a pre-equilibrium.

Our findings indicate the utility of K_d determinations in apportioning accurately the enthalpic and entropic contribution to ligand/protein binding. The results complement the structural information available through crystallography. The very low K_d of 4.5 nmol/L for VER-50589 against the human HSP90β is similar to that reported for radicicol (27). Thus, the isoxazole resorcinol VER-50589 is one of the most potent HSP90 ligands yet reported, exhibiting the tightest binding of any small molecule to be described in the literature to date.

The IC_{50} values obtained from the HSP90 ATPase assay and competitive binding assay also showed greater potency for VER-50589 over VER-49009, particularly in the case of the competitive binding assay where the difference was 2-fold. Note, however, that these differences were not as great as seen with the K_d values. VER-49009 and VER-50589 were over 40-fold more potent in both the ATPase and competitive binding assays when compared with 17-AAG and CCT018159 (27). The increase in HSP90 potency was translated into improved cellular activity. In the panel of human cancer cell lines, both VER-49009 and VER-50589 were 8- and 74-fold, respectively, more potent than CCT018159. In addition, the GI_{50} value of 78 ± 15 nmol/L for VER-50589 in the HCT116 human colon cells compares quite favorably with those for 17-AAG (16 ± 1 nmol/L; ref. 27) and radicicol (25.0 ± 1.2 nmol/L).[6]

The isoxazole VER-50589 showed greater antiproliferative potency than the corresponding pyrazole VER-49009. This difference was 9-fold when the mean values across the cancer cell line panel were compared. The greater cellular potency of VER-50589 may be attributed to the lower K_d for HSP90 binding and the increase in cellular accumulation. Exchanging the nitrogen of the pyrazole for the oxygen of the isoxazole in a range of analogues leads to a fall in the ClogP of between 0.1 and 0.4 unit along with a decrease in the polar space area (PSA) of 3 $Å^2$. The ClogP estimation indicates that the isoxazole VER-50589 is marginally less lipophilic than the pyrazole VER-49009. On the other hand, PSA has been shown to correlate well with membrane permeability (53). Thus, the slightly lower PSA value for VER-50589 may indicate an increase in membrane permeability over VER-49009, providing an explanation (perhaps together with increased HSP90 affinity) for the better cellular uptake of the isoxazole.

Metabolism to glucuronides leading to reduced accumulation explains the lower activity of both VER-50589 and VER-49009 in HT29 cells, as seen for CCT018159 (27). However, metabolism does not contribute to the greater uptake and potency of VER-50589 over VER-49009 in HCT116 cells as there is minimal glucuronide formation in this line that lacks uridine diphosphoglucuronosyltransferase enzymes.

Apart from HUVECs that were very sensitive, as with other HSP90 inhibitors and consistent with potential antiangiogenic activity (27, 35), the nontumorigenic epithelial cell lines (MCF10a, breast and PNT2, prostate) were generally more resistant to VER-49009 and VER-50589 than the tumor cells.

Using human melanoma cell lines with varying levels of NQO1, including an isogenic pair, we show here that the cellular activities of VER-49009 and VER-50589, like CCT018159 (27), are independent of NQO1. This is in contrast to 17-AAG, where cancer cell lines with high NQO1 levels were much more sensitive to 17-AAG due to the reduction of the quinone moiety to the more active hydroquinone metabolite (15, 16). Similarly, growth-inhibitory effects of another resorcinol-containing HSP90 inhibitor (radicicol) were similar in a different pair of isogenic cell lines, differing only in their NQO1 levels (16). The lack of the quinone moiety and the resulting independence from NQO1 removes a major source of variability in response, and potential toxicity, that is seen with 17-AAG (15). It also eliminates the potential for resistance developing via the loss of NQO1 expression. In addition, VER-49009 and VER-50589 were shown to retain activity in P-glycoprotein–mediated resistant cells (again in contrast to 17-AAG) and are able to circumvent resistance to oxaliplatin. However, the metabolism of the resorcinol moiety to glucuronides will confer potential resistance, as seen with HT29 human colon cancer cells (see above).

[6] Unpublished data.

Effects of VER-49009 and VER-50589 on the depletion of HSP90 client proteins *in vitro* were determined in human melanoma and breast cancer cell lines. These were selected as they are tumor types in which clinical activity has been reported with 17-AAG (46, 54). Like 17-AAG (15, 55) and CCT018159 (27), depletion of well-established HSP90 client proteins, such as ERBB2, cyclin-dependent kinase 4, and C-RAF, was observed. ERBB2 was consistently the most sensitive client. It was depleted as early as 8 h and at concentrations as low as $1 \times GI_{50}$ concentration of VER-50589. The depletion of C-RAF resulted in reduced ERK1/2 phosphorylation. In melanoma, activating oncogenic mutations in B-RAF, particularly the V600E form, are common (6). Interestingly, in contrast to previous results with 17-AAG (6, 7) and CCT018159 (27), both VER-49009 and VER-50589 were able to deplete wild-type B-RAF as effectively as mutant B-RAF. The reasons for this are unclear. Given that our HSP90 inhibitors deplete wild-type and mutant B-RAF and C-RAF (as well as A-RAF), it can be speculated that the therapeutic activity of these HSP90 inhibitors may be broader than that which has been predicted for MEK inhibitors (51).

The molecular chaperone HSP72 was induced following treatment with the HSP90 inhibitors. This is as predicted since HSP72 levels are mediated at least in part through the transcriptional activity of heat shock factor-1 (49), which is activated following HSP90 inhibition (56). HSP27 was also induced after treatment with VER-49009 and VER-50589. We previously reported up-regulation of HSP27 in other cell lines and also in tumor tissues obtained from patients receiving 17-AAG in a phase I clinical trial at our institution (52). Both HSP72 and HSP27 have cytoprotective roles (49), and the induction of these chaperones and stress proteins may reduce the apoptotic response to HSP90 inhibitors.

Survivin, which is involved in the inhibition of apoptosis and control of mitotic progression, is overexpressed in cancer and has been shown to require association with HSP90 for its stability and function (57). Knockdown of survivin expression by small interfering RNA enhances the response to 17-AAG (58). VER-49009 and VER-50589 were shown to deplete survivin in all the cell lines tested.

Using proteomic analysis, we discovered that expression of the protein arginine methyltransferase PRMT5 was decreased by 17-AAG in human cancer cell lines (52). PRMT5 was shown to be a novel HSP90-binding partner and potential client protein. VER-49009 and VER-50589 caused depletion of PRMT5 in human cancer cells. Because PRMT5 methylates proteins, including histones, and negatively regulates expression of the *ST7* and *NM23* tumor suppressor genes (59), it has been speculated that depletion of PRMT5 may contribute to the antitumor effects of HSP90 inhibition (52).

Like 17-AAG and CCT018159 (27), the pyrazole/isoxazole resorcinols caused marked accumulation in the G_1 and G_2-M cell cycle phases in HCT116 human colon cancer cells. We and others have shown that the nature of the cell cycle block is cell line and tumor type dependent (27, 36, 47). VER-49009 and VER-50589 also induce apoptosis at equivalent growth-inhibitory concentrations ($5 \times GI_{50}$ concentrations) in HCT116 cells.

As lead pyrazole/isoxazole resorcinols in our compound series, we wished to investigate VER-49009 and VER-50589 for their potential to provide the first indication of *in vivo* activity with such HSP90 inhibitors. To do this, we initially investigated pharmacokinetic properties in mouse plasma. The conduct of these studies was underpinned by our previous experience with cassette and individual compound dosing pharmacokinetic studies with CCT018159 and other early pyrazole compounds in mice (28). Based on the plasma levels achieved and the greater potency and cellular uptake of VER-50589 discussed earlier, we selected this isoxazole resorcinol to evaluate tumor tissue uptake, to obtain evidence of HSP90 inhibition in the tumor, and finally to gain an initial indication of the potential for antitumor activity.

Although plasma clearance of VER-50589 (and VER-49009) was rapid, the good cellular uptake properties of the isoxazole resulted in tumor levels in the HCT116 colon cancer xenograft that were above the *in vitro* GI_{50} for 24 h. Use of validated pharmacodynamic biomarkers of HSP90 inhibition confirmed that these exposures led to chaperone modulation in the tumor. *In vivo* tumor cell uptake and HSP90 inhibition was also confirmed by the extent and duration of ERBB2 depletion with low doses of VER-50589 in an orthotopic human ovarian OVCAR3 carcinoma ascites model. Indeed, in this model, the superiority of VER-50589 over VER-49009, also seen in cell culture studies, was confirmed by client protein biomarker changes. Encouraged by these pharmacokinetic and pharmacodynamic results, we evaluated the effects of nine daily doses of 100 mg/kg i.p. VER-50589 in s.c. HCT116 human colon cancer xenografts. This resulted in a statistically significant reduction of ~30% in tumor volume and weight. Induction of HSP72 and depletion of ERBB2 and C-RAF were also observed in these tumors, consistent with HSP90 inhibition. These observations provide initial support for the *in vivo* antitumor potential of the compound series.

The oral bioavailability of a group of diaryl pyrazole resorcinol compounds studied previously ranged from 1.8% for CCT018159 to 29.6% for CCT066965 (28).

In conclusion, we have shown promising biological properties for two selected examples of our diaryl resorcinylic pyrazole/isoxazole amide series of HSP90 inhibitors. Both showed an improvement in potency on the HSP90 target and in cells compared with the original lead compound CCT018159 (27, 29). Although the X-ray crystal structures showed an essentially identical binding mode in the NH_2-terminal ATP site of human HSP90α, the isoxazole VER-50589 exhibited tighter binding to the target compared with the corresponding pyrazole VER-49009, an effect attributable to enthalpy considerations. The high binding affinity of VER-50589 is similar to that of the potent natural product resorcinol radicicol. To our knowledge, the

isoxazole exhibits the strongest binding affinity yet reported for a small molecule HSP90 inhibitor. In addition, VER-50589 also showed improved cellular uptake over VER-49009. It seems likely that the higher binding affinity and improved cellular uptake are responsible for the greater cellular potency of VER-50589 over VER-49009. VER-50589, with average antiproliferative potency of 78 nmol/L in cancer cells, quite similar to the value of 25 nmol/L in a similar cancer cell panel for the clinical drug 17-AAG, is one of the most potent small molecule HSP90 inhibitors disclosed to date. In structure-activity studies to be reported elsewhere, we have shown that the enhanced cellular potency of the resorcinylic diarylisoxazole versus diarylpyrazole amides is a general feature of the isoxazole analogues. Molecular biomarker changes were consistent with HSP90 inhibition as was the induction of cell cycle arrest, cytostasis, and apoptosis. Pharmacokinetic and pharmacodynamic studies led to what is, to our knowledge, the first published demonstration of antitumor activity of this particular chemotype in an animal model. Thus, the diarylisoxazole VER-50589 is a promising advanced stage lead in the development of our diarylpyrazole/isoxazole amide series. Advantages of this type of agent over 17-AAG include better water solubility, lack of the quinone moiety that may be involved in hepatoxicity, and independence from the effects of metabolism by NQO1 and from P-glycoprotein. Further refinement of the structure will be carried out to fully optimize pharmacokinetic and pharmacodynamic properties and to enhance the antitumor activity of this promising new class of HSP90 inhibitors.

Acknowledgments

We thank many colleagues in the Chaperone Project Team and Signal Transduction and Molecular Pharmacology Team at The Institute of Cancer Research and also at Vernalis Ltd. for stimulating discussions and the Structural Chemistry groups at The Institute of Cancer Research and Vernalis Ltd. for help with the spectroscopic studies.

References

1. Maloney A, Workman P. HSP90 as a new therapeutic target for cancer therapy: the story unfolds. Expert Opin Biol Ther 2002;2:3 – 24.

2. Whitesell L, Lindquist SL. HSP90 and the chaperoning of cancer. Nat Rev Cancer 2005;5:761 – 72.

3. Hanahan D, Weinberg RA. The hallmarks of cancer. Cell 2000;100: 57 – 70.

4. Workman P. Combinatorial attack on multistep oncogenesis by inhibiting the Hsp90 molecular chaperone. Cancer Lett 2004;206: 149 – 57.

5. da Rocha DS, Friedlos F, Light Y, et al. Activated B-RAF is an Hsp90 client protein that is targeted by the anticancer drug 17-allylamino-17-demethoxygeldanamycin. Cancer Res 2005;65:10686 – 91.

6. Grbovic OM, Basso AD, Sawai A, et al. V600E B-Raf requires the Hsp90 chaperone for stability and is degraded in response to Hsp90 inhibitors. Proc Natl Acad Sci U S A 2006;103:57 – 62.

7. Kamal A, Thao L, Sensintaffar J, et al. A high-affinity conformation of Hsp90 confers tumour selectivity on Hsp90 inhibitors. Nature 2003;425: 407 – 10.

8. Obermann WM, Sondermann H, Russo AA, Pavletich NP, Hartl FU. *In vivo* function of Hsp90 is dependent on ATP binding and ATP hydrolysis. J Cell Biol 1998;143:901 – 10.

9. Panaretou B, Prodromou C, Roe SM, et al. ATP binding and hydrolysis are essential to the function of the Hsp90 molecular chaperone *in vivo*. EMBO J 1998;17:4829 – 36.

10. Schulte TW, An WG, Neckers LM. Geldanamycin-induced destabilization of Raf-1 involves the proteasome. Biochem Biophys Res Commun 1997;239:655 – 9.

11. Connell P, Ballinger CA, Jiang J, et al. The co-chaperone CHIP regulates protein triage decisions mediated by heat-shock proteins. Nat Cell Biol 2001;3:93 – 6.

12. Supko JG, Hickman RL, Grever MR, Malspeis L. Preclinical pharmacologic evaluation of geldanamycin as an antitumor agent. Cancer Chemother Pharmacol 1995;36:305 – 15.

13. Agatsuma T, Ogawa H, Akasaka K, et al. Halohydrin and oxime derivatives of radicicol: synthesis and antitumor activities. Bioorg Med Chem 2002;10:3445 – 54.

14. Egorin MJ, Lagattuta TF, Hamburger DR, et al. Pharmacokinetics, tissue distribution, and metabolism of 17-(dimethylaminoethylamino)-17-demethoxygeldanamycin (NSC 707545) in CD2F1 mice and Fischer 344 rats. Cancer Chemother Pharmacol 2002;49:7 – 19.

15. Kelland LR, Sharp SY, Rogers PM, Myers TG, Workman P. DT-Diaphorase expression and tumor cell sensitivity to 17-allylamino, 17-demethoxygeldanamycin, an inhibitor of heat shock protein 90. J Natl Cancer Inst 1999;91:1940 – 9.

16. Guo W, Reigan P, Siegel D, et al. Formation of 17-allylamino-demethoxygeldanamycin (17-AAG) hydroquinone by NAD(P)H:quinone oxidoreductase 1: role of 17-AAG hydroquinone in heat shock protein 90 inhibition. Cancer Res 2005;65:10006 – 15.

17. Glaze E, Smith A, Johnson D, et al. Dose range-finding toxicity studies of 17-DMAG. Proceedings of American Association of Cancer Research 2003;44:162 – 3.

18. Sydor JR, Normant E, Pien CS, et al. Development of 17-allylamino-17-demethoxygeldanamycin hydroquinone hydrochloride (IPI-504), an anti-cancer agent directed against Hsp90. Proc Natl Acad Sci U S A 2006;103:17408 – 13.

19. Soga S, Shiotsu Y, Akinaga S, Sharma SV. Development of radicicol analogues. Curr Cancer Drug Targets 2003;3:359 – 69.

20. Sharp S, Workman P. Inhibitors of the HSP90 molecular chaperone: current status. Adv Cancer Res 2006;95:323 – 48.

21. Janin YL. Heat shock protein 90 inhibitors. A text book example of medicinal chemistry? J Med Chem 2005;48:7503 – 12.

22. Chiosis G, Rodina A, Moulick K. Emerging Hsp90 inhibitors: from discovery to clinic. Anticancer Agents Med Chem 2006;6:1 – 8.

23. Roe SM, Prodromou C, O'Brien R, et al. Structural basis for inhibition of the Hsp90 molecular chaperone by the antitumor antibiotics radicicol and geldanamycin. J Med Chem 1999;42:260 – 6.

24. Chiosis G. Discovery and development of purine-scaffold Hsp90 inhibitors. Curr Top Med Chem 2006;6:1183 – 91.

25. Chiosis G, Caldas LE, Solit D. Heat shock protein-90 inhibitors: a chronicle from geldanamycin to today's agents. Curr Opin Investig Drugs 2006;7:534 – 41.

26. Cheung KM, Matthews TP, James K, et al. The identification, synthesis, protein crystal structure and *in vitro* biochemical evaluation of a new 3,4-diarylpyrazole class of Hsp90 inhibitors. Bioorg Med Chem Lett 2005;15:3338 – 43.

27. Sharp SY, Boxall K, Rowlands M, et al. *In vitro* biological characterization of a novel, synthetic diaryl pyrazole resorcinol class of heat shock protein 90 inhibitors. Cancer Res 2007;67: 2206 – 16.

28. Smith NF, Hayes A, James K, et al. Preclinical pharmacokinetics and metabolism of a novel diaryl pyrazole resorcinol series of heat shock protein 90 inhibitors. Mol Cancer Ther 2006;5:1628 – 37.

29. Dymock BW, Barril X, Brough PA, et al. Novel, potent small-molecule inhibitors of the molecular chaperone Hsp90 discovered through structure-based design. J Med Chem 2005;48:4212 – 5.

30. Drysdale M, Dymock B, Finch H, et al. Isoxazole compounds as inhibitors of heat shock proteins. 2004; pp. 1 – 180. [Eur. Pat. Off. No. WO 2004/072051 A1].

31. Wright L, Barril X, Dymock B, et al. Structure-activity relationships in purine-based inhibitor binding to HSP90 isoforms. Chem Biol 2004;11: 775 – 85.

32. Panaretou B, Siligardi G, Meyer P, et al. Activation of the ATPase

activity of hsp90 by the stress-regulated cochaperone aha1. Mol Cell 2002;10:1307 – 18.

33. Rowlands MG, Newbatt YM, Prodromou C, et al. High-throughput screening assay for inhibitors of heat-shock protein 90 ATPase activity. Anal Biochem 2004;327:176 – 83.

34. Howes R, Barril X, Dymock BW, et al. A fluorescence polarization assay for inhibitors of Hsp90. Anal Biochem 2006;350:202 – 13.

35. Sanderson S, Valenti M, Gowan S, et al. Benzoquinone ansamycin heat shock protein 90 inhibitors modulate multiple functions required for tumor angiogenesis. Mol Cancer Ther 2006;5:522 – 32.

36. Hostein I, Robertson D, DiStefano F, Workman P, Clarke PA. Inhibition of signal transduction by the Hsp90 inhibitor 17-allylamino-17-demethoxygeldanamycin results in cytostasis and apoptosis. Cancer Res 2001;61: 4003 – 9.

37. Workman P, Twentyman P, Balkwill F, et al. United Kingdom Co-ordinating Committee on Cancer Research guidelines for the welfare of animals in experimental neoplasia. 2nd ed. Br J Cancer 1998;77:1 – 10.

38. Raynaud FI, Whittaker SR, Fischer PM, et al. *In vitro* and *in vivo* pharmacokinetic-pharmacodynamic relationships for the trisubstituted aminopurine cyclin-dependent kinase inhibitors olomoucine, bohemine and CYC202. Clin Cancer Res 2005;11:4875 – 87.

39. Eccles SA, Court WJ, Box GA, et al. Regression of established breast carcinoma xenografts with antibody-directed enzyme prodrug therapy against c-erbB2 p185. Cancer Res 1994;54:5171 – 7.

40. Belotti D, Paganoni P, Manenti L, et al. Matrix metalloproteinases (MMP9 and MMP2) induce the release of vascular endothelial growth factor (VEGF) by ovarian carcinoma cells: implications for ascites formation. Cancer Res 2003;63:5224 – 9.

41. Hardcastle A, Boxall K, Richards J, et al. Solid-phase immunoassays in mechanism-based drug discovery: their application in the development of inhibitors of the molecular chaperone heat-shock protein 90. Assay Drug Dev Technol 2005;3:273 – 85.

42. Cummings J, McArdle CS. Studies on the *in vivo* disposition of Adriamycin in human tumours which exhibit different responses to the drug. Br J Cancer 1986;53:835 – 8.

43. Sharp SY, Kelland LR, Valenti MR, et al. Establishment of an isogenic human colon tumor model for NQO1 gene expression: application to investigate the role of DT-diaphorase in bioreductive drug activation *in vitro* and *in vivo*. Mol Pharmacol 2000;58:1146 – 55.

44. Sharp SY, Rowlands MG, Jarman M, Kelland LR. Effects of a new antioestrogen, idoxifene, on cisplatin- and doxorubicin-sensitive and -resistant human ovarian carcinoma cell lines. Br J Cancer 1994;70:409 – 14.

45. Sharp SY, O'Neill CF, Rogers P, Boxall FE, Kelland LR. Retention of activity by the new generation platinum agent AMD0473 in four human tumour cell lines possessing acquired resistance to oxaliplatin. Eur J Cancer 2002;38:2309 – 15.

46. Banerji U, O'Donnell A, Scurr M, et al. Phase I pharmacokinetic and pharmacodynamic study of 17-allylamino, 17-demethoxygeldanamycin in patients with advanced malignancies. J Clin Oncol 2005;23:4152 – 61.

47. Munster PN, Basso A, Solit D, Norton L, Rosen N. Modulation of Hsp90 function by ansamycins sensitizes breast cancer cells to chemotherapy-induced apoptosis in an RB- and schedule-dependent manner. See: E. A. Sausville, Combining cytotoxics and 17-allylamino, 17-demethoxygeldanamycin: sequence and tumor biology matters. Clin Cancer Res 2001;7:2155 – 8, 2228 – 36.

48. Hickey E, Brandon SE, Potter R, et al. Sequence and organization of genes encoding the human 27 kDa heat shock protein. Nucleic Acids Res 1986;14:4127 – 45.

49. Jolly C, Morimoto RI. Role of the heat shock response and molecular chaperones in oncogenesis and cell death. J Natl Cancer Inst 2000;92: 1564 – 72.

50. Sato S, Fujita N, Tsuruo T. Modulation of Akt kinase activity by binding to Hsp90. Proc Natl Acad Sci U S A 2000;97:10832 – 7.

51. Solit DB, Garraway LA, Pratilas CA, et al. BRAF mutation predicts sensitivity to MEK inhibition. Nature 2006;439:358 – 62.

52. Maloney A, Clarke P, Naaby-Hansen S, et al. Gene and protein expression profiling of human ovarian cancer cells treated with the HSP90 inhibitor 17-allylamino-17-demethoxygeldanamycin (17AAG). Cancer Res 2007;67:3239 – 53.

53. Palm K, Luthman K, Ungell AL, et al. Evaluation of dynamic polar molecular surface area as predictor of drug absorption: comparison with other computational and experimental predictors. J Med Chem 1998;41: 5382 – 92.

54. Modi S, Stopeck A, Gordon MS, et al. Phase I trial of KOS-953, a heat shock protein 90 inhibitor, and trastuzumab (T). J Clin Oncol (Meeting Abstracts) 2006;24:501.

55. Schulte TW, Neckers LM. The benzoquinone ansamycin 17-allylamino-17-demethoxygeldanamycin binds to HSP90 and shares important biologic activities with geldanamycin. Cancer Chemother Pharmacol 1998; 42:273 – 9.

56. Bagatell R, Paine-Murrieta GD, Taylor CW, et al. Induction of a heat shock factor 1-dependent stress response alters the cytotoxic activity of hsp90-binding agents. Clin Cancer Res 2000;6:3312 – 8.

57. Fortugno P, Beltrami E, Plescia J, et al. Regulation of survivin function by Hsp90. Proc Natl Acad Sci U S A 2003;100:13791 – 6.

58. Paduano F, Villa R, Pennati M, et al. Silencing of survivin gene by small interfering RNAs produces supra-additive growth suppression in combination with 17-allylamino-17-demethoxygeldanamycin in human prostate cancer cells. Mol Cancer Ther 2006;5:179 – 86.

59. Pal S, Vishwanath SN, Erdjument-Bromage H, Tempst P, Sif S. Human SWI/SNF-associated PRMT5 methylates histone H3 arginine 8 and negatively regulates expression of ST7 and NM23 tumor suppressor genes. Mol Cell Biol 2004;24:9630 – 45.